Scanning tunneling microscopy and spectroscopy of sodium-chloride overlayers on the stepped Cu(311) surface: Experimental and theoretical study

F. E. Olsson and M. Persson
Dept. of Applied Physics, Chalmers/Göteborg University, S-41296 Göteborg, Sweden.

J. Repp and G. Meyer
IBM Research, Zurich Research Laboratory, CH-8803 Rüschlikon, Switzerland

(Dated: February 2, 2008)

The physical properties of ultrathin NaCl overlayers on the stepped Cu(311) surface have been characterized using scanning tunneling microscopy (STM) and spectroscopy, and density functional calculations. Simulations of STM images and differential conductance spectrum were based on the Tersoff-Hamann approximation for tunneling with corrections for the modified tunneling barrier at larger voltages and calculated Kohn-Sham states. Characteristic features observed in the STM images can be directly related to calculated electronic and geometric properties of the overlayers. The measured apparent barrier heights for the mono-, bi-, and trilayers of NaCl and the corresponding adsorption-induced changes in the work function, as obtained from the distance dependence of the tunneling current, are well reproduced by and understood from the calculated results. The measurements revealed a large reduction of the tunneling conductance in a wide voltage region, resembling a band gap. However, the simulated spectrum showed that only the onset at positive sample voltages may be viewed as a valence band edge, whereas the onset at negative voltages is caused by the drastic effect of the electric field from the tip on the tunneling barrier.

PACS numbers: 68.35.Ct, 68.55.Ac, 68.37.Ef

I. INTRODUCTION

Thin films of insulating materials on metal surfaces are of direct technological interest in microelectronics, catalysis and as a corrosive protection. They are also attracting increasing interest for nanoscience and nanotechnology as potential substrates for atomic and molecular manipulation by the scanning tunneling microscope. In particular, this interest stems from the possibility to decrease the electronic interaction of assembled molecules and adatoms with the metal support. The non-vanishing electron density that reaches through the ultrathin insulating films, thickness below 1 nm, allows for these surfaces to be studied by means of STM[1,2,3]. A most important prerequisite for the realization of this possibility is to be able to grow stable and atomically thin insulating films on metal surfaces with a well-characterized and ordered geometric structure. So far the number of systems studied that fulfills these conditions have been very limited[4]. One interesting candidate is provided by NaCl overlayers on a stepped Cu(311) surface, which we have studied in detail by scanning tunneling microscopy (STM) [5] and also most recently by density functional calculations[6].

These experimental and theoretical studies revealed several interesting aspects of the growth, structure and bonding of these systems. The initial growth of NaCl on the Cu(311) surface was found to be two dimensional and commensurate. The lattice match of the overlayer with the substrate was suggested in the experimental study to be stabilized by the incomplete screening of the step Cu atoms resulting in an electrostatic interaction between these atoms and the Cl atoms. Density functional calculations corroborated this suggestion and showed also that the bonding of the overlayer on the surface was further stabilized by the formation of a weak chemical bond between the step Cu atoms and the Cl stoms. These calculations revealed also large relaxations of the monolayers such as a buckling of the layer with a large influence on the work function. These results call for a detailed scanning tunneling microscopy study of the topography of and the tunneling conductance through these overlayers. In particular, the imaging of insulating overlayers on metal surfaces for biases well below 1 V has not been studied before.

In this paper, we present atomically resolved topographical images of NaCl mono-, bi- and tri-layers on Cu(311) obtained by an STM and discuss them in relation to simulated images based on density functional calculations and the Tersoff-Hamann (TH) approximation[7]. In this approximation, STM images and scanning tunneling spectra are obtained from the local density of states (LDOS) at the position of the tip apex. The conductivity of the sample are further investigated using scanning tunneling spectroscopy. The measured $\frac{dI}{dV}$ spectra are compared with simulated spectra and discussed in relation to the energy dependence of the calculated LDOS. This study includes also a calculation and discussion of the apparent heights and work functions of these layers obtained from tunneling measurements. The apparent height of an NaCl overlayer contains information about the "local" work function, that is, the tunneling barrier. The tunneling barriers are obtained from the measured distance dependence of the tunneling conductance.

STM investigations of insulating overlayers provide important information about the growth mechanisms and

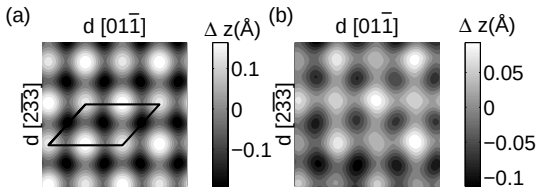

FIG. 1: Experimental STM images and calculated LDOS images of a NaCl monolayer in the p(3x2)-II structure. (a) Calculated LDOS image at an average distance of 7.9 Å from the Cu(311) surface. The surface unit cell used in the calculation, see Fig. 5 (right), is indicated. (b) Experimental STM image with tunneling parameters 210pA and -24meV. In both (a) and (b) the presented area is 15x15Å^2.

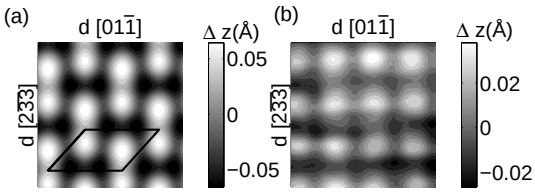

FIG. 2: Experimental STM images and calculated LDOS images of a NaCl bilayer on Cu(311). (a) Calculated LDOS image at an average distance of 9.0Å from the Cu(311) surface. The surface unit cell used in the calculation, see Fig. 5 (left), is indicated. (b) Experimental STM image with tunneling parameters 360pA and -100meV. In both (a) and (b) the presented area is 15x15Å^2.

the local electronic structure of the overlayer. In earlier STM investigations of ultrathin insulating overlayers on metal surfaces such as MgO on Ag(100)[2] and NaCl on Al(111) and Al(100)[1] the experiments were carried out at relatively high biases of about 1eV to provide atomic resolution of the overlayer. Atomically resolved STM images have also been observed for NaCl layers on Ge(100)[8], where only one type of atoms was found to be imaged as a protrusion[1]. A combined STM and density functional study of NaCl layers on an Al(111) and Al(100) surface revealed that only the Cl atoms were imaged as protrusions. In this work, the atomic contrast as well as the apparent height of the NaCl layers was discussed by comparing the experimental images with calculations of LDOS within the TH approximation. MgO layers on an Ag(100) surface were studied using measured $\frac{dI}{dV}$ spectroscopy and the band gap of the bulk MgO electronic structure was found to be developed within the first three monolayers[2]. This finding was corroborated by density functional calculatrions of the energy dependence of the LDOS within the MgO layers.

The paper is organized as follows. In section II our experimental STM and $\frac{dI}{dV}$ results for mono-, bi- and trilayers of NaCl on Cu(311) are presented. In section III we present the geometric and electronic structure and simulated STM images and $\frac{dI}{dV}$ spectra for the same systems. The experimental and theoretical results are compared and discussed in Section IV. Finally, section V concludes the paper.

II. EXPERIMENTAL METHODS AND RESULTS

Our experiments were carried out with a low temperature scanning tunneling microscope[9], operated at 13K. We used a chemomechanically polished Cu(311) single crystal, which was cleaned by Ne^+ sputtering and annealing at 750K. NaCl was evaporated thermally and the deposition and annealing temperature was varied in the range of 400K-570K. In this temperature range Cu surface atoms are mobile. As an STM tip we used an electrochemically etched tungsten wire. Bias voltages refer to the sample voltage with respect to the tip. The STM images were taken at 13K. The STM images for mono- and bi-layers that are presented in Figs. 1(b)-2(b) and bare Cu(311) were acquired at relatively low voltages of $\mid V \mid \leq$ 100mV, being well within the band gap of bulk NaCl. For the bare Cu(311) and the monolayer structures our experimental images were obtained under identical tunneling conditions, that is, both applied current and voltage, and tip were identical. Since the growth of the first layer was always completed before the formation of the second layer we could not be sure that the tip structure was identical in the imaging of the bare and the bilayer covered surfaces as for the bare and monolayer-covered surfaces. However, we could simultaneously record STM images of islands with one to three layers on top of the monolayer. Up to four layers of NaCl could be imaged with atomic resolution.

In our experiments we observe two different structures for the NaCl monolayer, shown in Figs. 1(b) and 3(b). As argued in our earlier study, we attribute these images to be associated with the structures presented in Fig. 5. Here we follow the notation of Ref.[6] and designate these structures as p(3x2)-II and p(3x2)-I, respectively[24]. In the STM images of these structures, we identify one characteristic feature for each structure. In the STM image of the p(3x2)-II structure every second protrusion appear slightly brighter. For the p(3x2)-I structure we note a slight tendency for the protrusions to group into pairs, even though, this effect is small and is just at the limit of the present resolution. In contrast to the monolayer, atomically resolved STM images of the bi- and trilayers (Fig. 2(b)) did not show any differences between the domains corresponding to p(3x2)-I and -II structures, although it could be concluded that both these domains are present with the help of characteristic defects, consisting of a missing Cu atoms in the topmost substrate layer[5].

The apparent heights, Δz_l, of the NaCl overlayers ($l = 1, 2, 3$ for the mon-, bi-, and tri-layer) are presented in Table I. Δz_l is defined as the vertical change in tip position when a step edge is scanned. We find that Δz_l

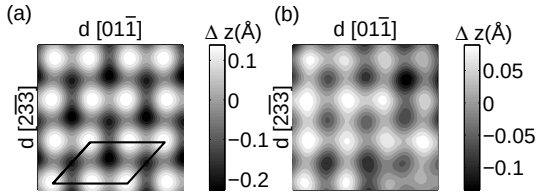

FIG. 3: Experimental STM images and calculated LDOS images of a NaCl monolayer in the p(3x2)-I structure. (a) Calculated LDOS image at an average distance from the Cu(311) surface of 7.9 Å. The surface unit cell used in the calculation, see Fig. 5 (left), is indicated. (b) Experimental STM image with tunneling parameters 210pA and -24meV. In both (a) and (b) the presented area is 15x15Å^2.

TABLE I: Calculated work function $\Phi_{\rm theory}$ and experimentally measured mean barrier height $\overline{\Phi}_{\rm exp.}$ of NaCl layers on Cu(311). The values in brackets indicate the relative changes with respect to the clean copper surface. Δz_l are the apparent heights obtained from LDOS calculations (theory) and STM experiments (exp) and $\Delta z_l^{geom.}$ are the calculated geometric height. l=1,2 and 3 for mono-, bi- and trilayers, respectively. The result for the NaCl monolayer is for the p(3x2)-II structure.

	Cu(311)	mono	bi	tri
$\Phi_{\rm theory}$ (eV)	4.31	3.53 (-18%)	2.85 (-34%)	2.83 (-34%)
$\overline{\Phi}_{\rm exp.}$(eV)	3.81	3.23 (-15%)	2.82 (-26%)	2.82 (-26%)
Δz_l (exp) (Å)		1.6	1.4	1.3
Δz_l (theory) (Å)		1.8	1.1	-
$\Delta z_l^{\rm geom.}$ (Å)		2.5	2.8	2.8

decreases with l and is positive for all l. As also shown in Table I, the geometric heights, $\Delta z_l^{\rm geom}$, of the NaCl overlayers are about 1Å larger than Δz_l. This implies that the tip-surface distance decrease with l.

To quantify work function changes upon adsorption of NaCl layers, we have carried out measurements of the distance dependence of the tunneling current I[10]. The feed-back loop was switched off and a voltage ramp was applied to the z-piezo drive while measuring the current I as a function of tip-sample distance z. The resulting sweep in z measured 2.7 Å in height and had a duration of about one second. The resulting current curve followed closely an exponential dependence, $I(z) \propto \exp(-2\kappa z)$ from which an apparent barrier height $\overline{\Phi}$ was defined from the decay constant κ as $\overline{\Phi} = \hbar^2\kappa^2/(2m_e)$. The relationship between $\overline{\Phi}$ and the work function Φ of the sample is not straightforward and has been discussed at length in the literature[11,12]. The systematic deviation of $\overline{\Phi}$ from Φ decreases with increasing tip-surface distance, corresponding to a larger vacuum region between the tip and the sample. So this deviation was minimized by recording spectra at a lowest possible current, ranging down to 10pA, so as to maximize the tip-surface distance. Although Φ can not be determined directly, the adsorption-induced relative changes in $\overline{\Phi}$ are expected to correspond to the relative changes in Φ. The experimental uncertainty in determining $\overline{\Phi}$ from κ is set by the vertical length scale calibration, being a few percent. Using this procedure, we find that the measured work function difference between a NaCl monolayer and the clean surface agrees well with the work function difference measured by an atomic force microscopy tip[13].

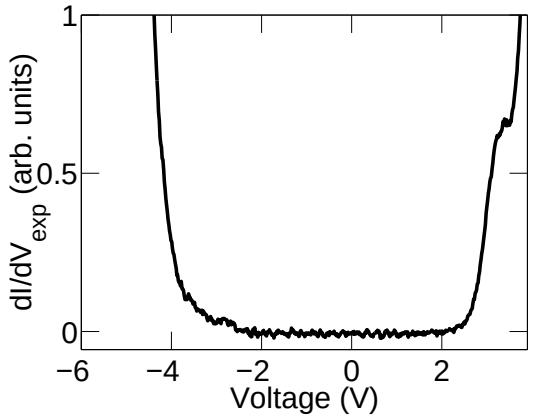

FIG. 4: Experimental dI/dV spectrum for a monolayer NaCl on Cu(311). The tip-sample distance corresponds to a current setpoint of I = 0.3 nA at V = 3.8 V. This distance is by about 6 Å larger than the distance for the imaging parameter set used in the Figs. 1 and 3.

The apparent barrier height $\overline{\Phi}$ for the bare surface and NaCl overlayers deduced from the measured the $I(z)$ are shown in Table I. These results show that there is a substantial decrease in $\overline{\Phi}$ upon adsorption of the first layer and an even larger decrease for the second. No further changes of $\overline{\Phi}$ are observed for the thicker layers. This result indicates that the nature of the monolayer differ from the interface layer in the multilayers.

The insulating properties of the monolayer have been investigated using dI/dV spectroscopy, shown in Fig. 4 for a monolayer. When acquiring the spectra the tip was retracted about 6Å. The spectra is not sensitive to the tip position relative to the surface. The poor conductivity of the monolayer is manifested by a very small tunneling current between -4 and +3V and exponential off and onsets of $\frac{dI}{dV}$ at these voltages. The other characteristic feature in the spectra is the shoulder at about +3.2V.

III. THEORETICAL METHODS AND RESULTS

The results obtained from the STM measurements for the bare surface and the NaCl overlayers such as constant current images, work functions and apparent heights have been analyzed by extending our recent density functional calculations of the electronic and geometric structures of these system[6], including now also the trilayer, to tunneling. These calculations were based on a plane wave basis set and the projector augmented wave (PAW) method[14,15] as implemented in the `VASP`[16] code. A generalized gradient approximation[17] was employed for

TABLE II: Calculated interface energies and geometrical parameters of a NaCl monolayers, bilayer and trilayer on the (311) surface of Cu. The interface layer for the bilayer and trilayer correspond the p(3x2)-I structure. The adsorption energy, E_a, is given in eV per NaCl pair of the interface and is defined as $E_a = (E_{lNaCl/Cu} - E_{nNaCl} - E_{(l-n)NaCl/Cu})/\mathrm{m}$, where l is the number of NaCl layers in the overlayer, m is the number of NaCl in the interface and n=1, n=1,2 and n=1,2,3, for monolayers, bilayers and trilayers, respectively. $\Delta b = z_{Cl} - z_{Na}$, where z_{Cl} and z_{Na} are the coordinates of Na and Cl atoms perpendicular to the surface. z_{Cl} is the distance between the Cl atom and the Cu surface layer. d_{Cl-Cl} is a Cl–Cl distance along a row in the layer. The distance between Cl atoms on two neighbouring Cu-rows is 4.26 Å. The superscripts (t) and (b) for the p(3x2)-I structure corresponds to Cl atoms in top and bridge sites relative to the top Cu(311) layer, respectively. The superscript (t') and (b') for the p(3x2)-II structures corresponds to Na atoms in top and bridge sites relative to the second Cu(311) layer, respectively. See Fig. 1 in Ref.[6].

	E_a (eV)	Δ b (Å)	z_{Cl} (Å)	d_{Cl-Cl}
monolayer				
p(3x2)-I	0.42	$0.31^{(t')}$, $0.35^{(b')}$	2.54	3.78, 3.94
p(3x2)-II	0.41	$0.36^{(t)}$, $0.29^{(b)}$	$2.56^{(t)}$ $2.49^{(b)}$	3.86, 3.86
bilayer				
interface	0.35	$0.13^{(t')}$, $0.11^{(b')}$	$2.50^{(t)}$	3.83, 3.89
top	0.22	< 0.02	5.29	3.86, 3.86
trilayer				
interface	0.34	$0.15^{(t')}$, $0.13^{(b')}$	2.51	3.83, 3.89
middle	0.25	-0.09	5.25	3.86, 3.86
top	0.31	0.08	8.14	3.86, 3.86

the exchange-correlation potential. The system was represented by a slab in a super cell geometry[25] and the equilibrium geometry was obtained by a structural optimization[26]. We considered the two p(3x2)-I and p(3x2)-II structures for the NaCl monolayer, shown in Fig. 5 and the structures for the bilayer and trilayer that were formed by adding subsequent NaCl layers on the p(3x2)-I structure of the monolayer. In Tables I and II, we show the calculated work functions and key bonding parameters for the NaCl layers. For easy reference these tables include also the parameters for monolayer and the bilayer, previously presented in Ref.[6]. The calculated partial s, p, and d density of states of the Cl atoms in trilayer are shown in Fig. 7. As expected, the width of the Cl peak is largest for the interface layer (Fig. 7(c)) and smallest for the outermost layer (Fig. 7(a)), due to larger overlap with the Cu states for the interface layer.

The STM images and the apparent heights of the overlayers were simulated using the Tersoff and Hamann (TH) approximation[7] for the tunneling current. In this approximation the tunneling current for low bias is proportional to the LDOS, $\rho(\mathbf{r_0}, \epsilon_F)$, of the surface at the position of the tip apex, $\mathbf{r}_0$. The LDOS was calculated from the Kohn-Sham wavefunctions, see Ref.[18] for details. The topographical STM images were obtained from the topography of the contours of constant $\rho(\mathbf{r_0}, \epsilon_F)$,

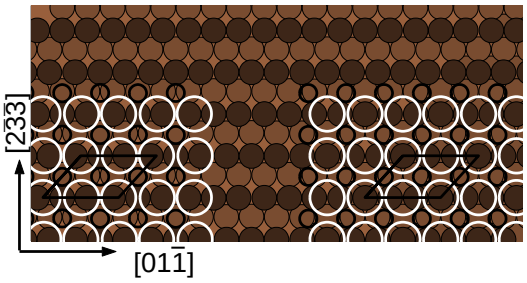

FIG. 5: Ordered structures of a NaCl monolayer on Cu(311): (left) p(3x2)-I and (right) p(3x2)-II. The dark and light filled circles represent Cu atoms of the first and second layer, respectively, and the large white and small black open circles represent Cl and Na atoms, respectively. The unit cells used in the calculations are indicated. In the p(3x2)-I structure all Cl atom sites are equivalent, whereas there are two inequivalent Na atom sites, top (t') and bridge (b'), with respect to the second Cu layer. In the p(3x2)-II all Na atom sites are equivalent, whereas there are two inequivalent Cl atom sites, top (t) and bridge (b) sites with respect to the first Cu layer, see also Fig. 1 in Ref.[6].

which henceforth will be referred to as LDOS images.

We have also simulated differential conductance, $\frac{dI}{dV}$ spectra, using the LDOS outside the surface. For these simulations it is necessary to consider the effects on the tunneling caused by the applied electric field from the tip. Following Lang[19], these effects are partly accounted for by calculating $\frac{dI}{dV}$ within the average tunneling barrier approximation as

$$\frac{dI}{dV} \propto \frac{d}{dV}\left(\int_{\epsilon_F}^{\epsilon_F+eV} \rho_S(\epsilon)T(\epsilon,V)d\epsilon\right) \quad (1)$$

$$= e\rho_S(\epsilon_F+eV)T(\epsilon_F+eV,V) + \int_{\epsilon_F}^{\epsilon_F+eV} \frac{d}{dV}(\rho_S(\epsilon)T(\epsilon,V))d\epsilon\,, \quad (2)$$

where $T(\epsilon, V)$ is the transmission coefficient through the average barrier for an electron with energy ϵ and is given by,

$$T(\epsilon,V) = \exp\left(-2s\sqrt{2m(\Phi_{av}+\epsilon_F-\epsilon+eV/2)}/\hbar\right) \quad (3)$$

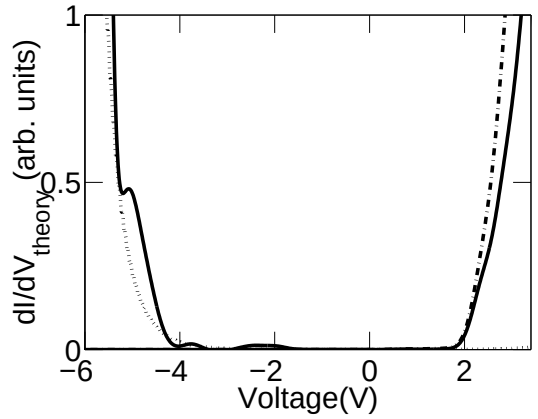

FIG. 6: Calculated $\frac{dI}{dV}$ spectra for a monolayer NaCl in the p(3x2)-I structure on Cu(311). The solid and dotted lines are calculated from Eq. (2) using the full energy dependence of $\rho_S(\epsilon)$ and a constant $\rho_S(\epsilon)$, $\rho_S(\epsilon) = \rho_S(\epsilon_F)$, respectively. The dashed-dotted line is the result obtained using only the local density of states contribution to $\frac{dI}{dV}$ (first term in Eq. (2)). In the calculations we used z_s = 2 Å, s = 10 Å and Φ_{av} = 3.5 eV.

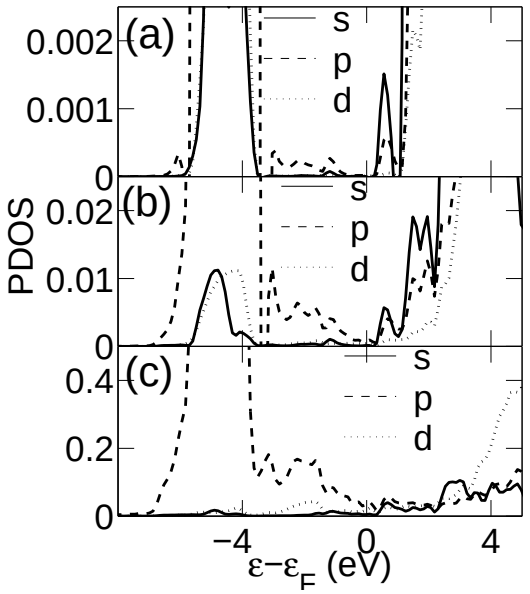

FIG. 7: Partial s, p and d density of states around Cl atoms in a NaCl trilayer on Cu(311). The Cl atom is in (a) the third (outermost) NaCl layer, (b) the second layer, and (c) the first (interface) layer. Note that the scale of the presented PDOS on the three Cl atoms differ by several orders of magnitude.

Here $\Phi_{av} = (\Phi_T + \Phi_S)/2$ where Φ_T and Φ_S is the tip and sample work function, respectively, $\rho_S(\epsilon)$ is the LDOS at a distance z_s just outside the surface layer defining the boundary of the vacuum region and s is the distance between z_s and the tip apex. The first term in Eq. (2) is the LDOS at the tip-apex taking into account electric field in the tunneling junction. In the limit of vanishing voltage only this term survives and the TH approximation is recovered. Note that this result for $\frac{dI}{dV}$ is well defined for $|V| < 2\Phi_{av}$ but the average barrier approximation breaks down for voltages approaching the field-emission regime, that is, for $V > \Phi_S/e$ or $V < -\Phi_T/e$.

In Fig. 6, we show the simulated $\frac{dI}{dV}$ spectra for a monolayer of NaCl in the p(3x2)-II structure. The behavior of $\frac{dI}{dV}$ in the voltage region -3 to 3 V is well understood from the behaviour of the LDOS. In particular, the rapid increase of $\frac{dI}{dV}$ around V = 2 V is an LDOS effect and may be viewed as conduction band edge. In contrast, the rapid decrease of $\frac{dI}{dV}$ around V = -4.5 V is not an LDOS effect associated with any valence band edge. Note that the large contribution of electron states of p or s character around the Cl atoms to the partial DOS in Fig. 7 in the corresponding energy region does not show up in the LDOS. As illustrated by the result for $\frac{dI}{dV}$ in Fig. 6, using an energy-independent $\rho_S(\epsilon) = \rho_S(\epsilon_F)$, the rapid decrease comes from the second term in Eq. (2), which describes the drastic effect of the voltage dependent barrier on the tunneling and the larger probability for tunneling of electrons with energies closer to the vacuum level at larger negative voltages. In the calculation we have used the same work function for the tip and the sample so we expect even a more dramatic onset of $\frac{dI}{dV}$ for V < -3.5 V corresponding to the field-emission regime.

IV. DISCUSSION

We begin by comparing and discussing the measured apparent barrier heights and calculated work functions for the p(3x2)-I monolayer, the bilayer and the trilayer. As shown in Table I, the calculated changes in work functions reproduce nicely the measured changes for the bare surface and its change upon adsorption of the overlayers. Note that the measured apparent barrier height and the calculated work function can not be compared directly. From the calculations we are able to understand the reduction of Φ upon adsorption and its layer dependence in terms of bonding and buckling of the monolayer. This explanation was discussed in detail in our previous study[6] and will only be summarized here.

In general, the surface contribution to Φ is determined by the surface dipole layer, which have contributions both from electronic and ion-core rearrangements upon adsorption. The reduction of Φ upon adsorption was argued to be caused by the formation of a weak chemical bond between the Cl atoms and the metal substrate and the screening of the Na^+ ion by the metal electrons. The substantially smaller reduction of Φ for the monolayer than for the bilayer and the trilayer is caused by the large buckling of the monolayer with a large inward relaxation of the Na^+ ions relative to the Cl^- ions, resulting in a dipole layer that increases the work function. This buckling is substantially reduced for the bilayer and the trilayer and the work function reductions for these layers are governed mostly by the electronic rearrangements, which

are limited to the interface region. The measured Φ is thus consistent with a buckling of the monolayer and an interface bonding that involves electron rearrangements between the overlayer and the substrate.

Next we turn to a comparison and a discussion of observed and simulated STM images for the bare surface and the overlayers. These images contain information about the surface electronic and geometric structure through the tails of the wave functions in the vacuum region. Since the TH approximation for the tunneling is not based on any detailed model for the tip s density of states, we are not able to determine the distance, z_0, between the tip apex and the surface Cu layer from the tunneling conductance. However, the bare surface and the two monolayers were imaged under identical tunneling conditions so we can use the image for the bare surface to calibrate the value of the $\rho(\mathbf{r_0}, \epsilon_F)$ in the calculation of the LDOS images and to make a prediction of the images for the monolayers.

For the bare Cu surface, the calculated LDOS image gives the same tip-surface corrugation across the Cu rows as the STM image at an average z_0 of about 6.1 Å. No corrugation could be resolved along the Cu rows, neither in the LDOS image nor in the STM image. In contrast to the flat single crystal metal surfaces for which the TH approximation fails to reproduce atomically resolved STM images[20], the measured tip-surface corrugation can be reproduced by a realistic value for z_0, for which the TH approximation should be applicable. For the flat metal surfaces, the imaging mechanism has been argued to involve a direct tip-surface interaction[21].

In Figs. 1 and 3, we show the calculated LDOS images for the investigated monolayers, using the same value of $\rho(\mathbf{r_0}, \epsilon_F)$ as for the bare surface that reproduced the observed surface corrugation. The corresponding average value of z_0 is 7.9 Å. The resulting LDOS images are in overall good agreement with the observed STM images although the corrugation is somewhat larger in the LDOS images than in the STM images. The LDOS images support our original interpretation of the observed STM images that the protrusions correspond to Cl atoms[5]. The dominant contribution from the states of the Cl atom to the tunneling is understood from the participation of the p states in the bond as indicated by the corresponding partial density of states in Fig. 7.

As shown in Fig. 1, the LDOS image for the p(3x2)-II monolayer reproduces nicely the experimental observation that every second Cl is imaged slightly brighter. In our calculations we attribute the brighter protrusions to be derived from Cl atoms at bridge sites. This difference in brightness corresponds to a difference in z_0 of about 0.054 Å and is consistent with larger adsorption height, z_{Cl}, of 0.07 Å (see Table II) for the Cl atoms at the bridge sites than at the top sites. However, the hybridization of the $3p$ states of the Cl atoms with the metal states at the Fermi level is found to be stronger for the top site than for the bridge site. This electronic effect counteracts in part the geometric effect on the tip-surface corrugation.

As shown in Fig. 3, the tendency of pairing of the protrusions in the STM image for the p(3x2)-I monolayer is well reproduced by the LDOS image. This pair formation reflects the geometric relaxations of the Cl atoms along the Cu rows, resulting in two different Cl–Cl distances, which differ by 0.16 Å (see Table II). However, the geometric relaxations contribute only a minor part to the difference in distance of about 0.9 Å between protrusions along the rows. So in this case the dominant part of this difference is an electronic structure effect associated with the tilting of the Cu–Cl bond and the hybridized $3p$ states of Cl with respect to the surface normal.

In comparing STM and LDOS images of the bilayer we cannot adopt the same unambiguous procedure for the choice of average z_0 as we used for the monolayers. The bare surface and the bilayer are never imaged under the same tunneling conditions because the monolayer is fully developed before the formation of the bilayer. However, in our comparison with the STM image we use the same value for $\rho(\mathbf{r_0}, \epsilon_F)$ as above, which corresponds to an average z_0 of 9.0 Å. As for the monolayers we find that the protrusions in the LDOS image for the bilayer shown in Fig. 2 correspond to Cl atoms. As shown in Fig. 7, there is still a contribution from Cl states to the partial DOS around the Fermi level. This contribution is much smaller than for the Cl atom in the interface layer but is compensated by the average distance of the tip from the outermost NaCl layer being only about 3.5 Å for the bilayer, which is about 2Å shorter than the corresponding distance for the monolayer with the same value of $\rho(\mathbf{r_0}, \epsilon_F)$. The agreement between the LDOS and STM image with respect to amplitude of the surface corrugation is about the same as for the two monolayers but in contrast to the STM image the protrusions are more diffuse and paired into dimers in the LDOS image. This pairing is a pure electronic structure effect because the distances between Cl atoms across the rows are the same even though the atoms are inequivalent. Note that the distance of about 3.5 Å between the tip and the outermost NaCl layer is slightly too short to justify the TH approximation and an enhancement of the contrast from tip-surface interaction cannot be ruled out[21]. In particular, the tip-surface distance is even shorter for the tri- and quadrolayers so the observed atomic resaolution might be caused by the tip-surface interactions being sensitive to the identity of the underlying atom.

The apparent heights Δz_l of the single steps on the NaCl multilayer l provide indirect information about the conductance through the layers. For example, Δz_l is equal to zero or the geometrical height for a multilayer l of vacuum or Cu, respectively. Because bulk NaCl is a wide-gap insulator with a calculated band gap of 5.0 eV[27], the electrons around the Fermi level have to tunnel through the film so its conductance should be substantially less than an Cu layer, resulting in a smaller apparent height than the geometrical height.

As shown in Table I, the calculated Δz_l are in good agreement with the experimentally measured Δz_l for the

mono- and bi- layers and are indeed appreciably smaller than their geometrical heights. In particular, we find that an adsorbed multilayer corresponds to a vacuum layer with an height being about half the geometrical height of the multilayer. The increasing difference in geometrical height and apparent heights with the number of layers makes it increasingly difficult to image the layer. The larger Δz_1 than Δz_l for $l > 1$ is consistent with the behavior of the calculated partial s, p, and d DOS around the Cl atoms, as shown in Fig. 7. The interface layer has the largest conductivity because of the formation of a weak covalent bond between a Cl atom in the interface layer and the Cu substrate results in a non-vanishing density of states in the gap region in the interface layer. Whereas for the other layers, this contribution to the density of states are vanishingly small resulting in a smaller conductance and smaller apparent heights than for the interface layer. Note that the variation of the the work functions with the number of adsorbed layers contribute to Δz_l but cannot explain the variation in Δz_l with l. For instance, the decrease of the work function from the monolayer to the bilayer decreases the difference between Δz_1 and Δz_2 because wave functions for electrons at the Fermi level decreases more slowly with decreasing work function.

Finally, how the tunneling through a NaCl overlayer is affected by the presence of a band gap in bulk NaCl is obtained from the measured $\frac{dI}{dV}$ spectrum. The characteristic features of this spectrum such as the strong reduction of $\frac{dI}{dV}$ for voltages in the range from -4.5 to 2 V is reproduced rather well by the simulated $\frac{dI}{dV}$ spectrum. This drastic reduction suggests a depletion of the LDOS in the corresponding energy region, which can be attributed to the absence of propagating states in the overlayer in this energy region and the formation of a band gap. However, our discussion in Section III of the simulated $\frac{dI}{dV}$ spectrum in Figs. 6 showed that this suggestion is oversimplified. The onset at around $V = 2$ V is an LDOS effect whereas the onset at $V =$ -4.5 V is caused by the voltage-dependent barrier and field-emission[28].

V. CONCLUSIONS

In conclusion, we have carried out a combined scanning tunneling microscopy and density functional study of the surface topography, the apparent heights, work functions and the differential conductance of mono-, bi-, and trilayers of NaCl on a stepped Cu(311) surface. The experimental results are well reproduced by the calculations, which also provide physical insights and interpretation of the results. The adsorption-induced changes of electronic and geometric structure of the NaCl overlayer are found to be significant. The observed large adsorption-induced changes in the work function are found to be associated with substantial charge rearrangements upon adsorption. The Cl atoms were shown to be imaged as protrusions. In the STM images, also the different positions of the Cl atoms relative to the underlying Cu(311) lattice in the p(3x2)-I and p(3x2)-II structures of the NaCl monolayer were resolved. The poor conductivity of the layers were revealed by the apparent heights of steps being only half of the geometrical heights. Furthermore, $\frac{dI}{dV}$ spectra revealed a large reduction of the tunneling conductance in a wide voltage region, resembling a band gap. However, the simulated spectrum showed that only the onset at positive sample voltages may be viewed as a conduction band edge, whereas the onset at negative voltages is caused by the drastic effect of the electric field from the tip on the tunneling barrier.

Acknowledgements

We gratefully acknowledge partial funding by the EU-RTN project "AMMIST" and the Deutsche Forschungsgemeinschaft Project No. RI 472/3-2 (JR,GM). FO and MP are grateful for support from the Swedish Research Council (VR) and the Swedish Foundation for Strategic Research (SSF) through the materials consortium "ATOMICS". Allocations of computer resources through the Swedish National Allocations Committee (SNAC) and the Consortium of Heavy Computing (KTB) at Chalmers are also gratefully acknowledged.

[1] W. Hebenstreit, J. Redinger, Z. Horozova, M. Schmid, R. Podlucky and P. Varga, Surf. Sci **L321** (1999) L321
[2] S. Schintke, S. Messerli, M. Pivetta, F. Patthey, L. Libioulle, M. Stengel, A. DeVita and W D Schneider, Phys. Rev. Lett **87** (2001) 276801
[3] J. Libuda, F. Winkelmann, M. Bäumer, H. J. Freund, T. Bertams, N. Neddermeyer and K Müller, Surf. Sci., **318** (1994) 61
[4] M. Bäumer and H. J. Freund, Progr. Surf. Sci. **61** (1999) 127
[5] J. Repp, S. Fölsch, G. Meyer and K.-H. Rieder, Phys. Rev. Lett. **86** (2001) 252
[6] F. E. Olsson and M Persson, Surf. Sci. **540** (2003) 172
[7] J. Tersoff and D. R. Hamann, Phys. Rev. Lett. **50** (1983) 1998
[8] K. Glöckler, M. Sokolowski, A. Soukopp, E. Umbach, Phys. Rev. B **54** (1996) 7705
[9] G. Meyer, Rev. Sci. Instrum. **67** (1996) 2960

[10] G. Binnig, H. Rohrer, Ch. Gerber and E Weibel, Phys. Rev. Lett. **49** (1982) 57
[11] N. D. Lang, Phys. Rev. B **37** (1988) 10395
[12] L. Olesen, M. Brandbyge, M. R. Sørensen, K W Jacobsen, E. Lægsgaard, I. Stensgaard and F. Besenbacher, Phys. Rev. Lett. **76** (1996) 1485
[13] R. Bennewitz, M. Bemmaerlin, M. Guggisberg, C. Loppacher, A. Baratoff, E. Meyer, H.-J. Günterrodt, Surf. Interface Anal. **27** (1999) 462
[14] G. Kresse and D. Joubert, Phys. Rev. B **59** (1999) 1758
[15] P. E. Blöchl, Phys. Rev. B **50** (1994) 17953
[16] G. Kresse and J. Furthmüller, Phys. Rev. B **54** (1996) 11169
[17] J. P. Perdew, J. A. Chevary, S. H. Vosko, K. A. Jackson, M. R. Pederson, D. J. Singh and C. Fiolhais, Phys. Rev. B **46** (1992) 6671
[18] F. E. Olsson, N. Lorente, M. Persson, L. J. Lauhon and W. Ho, J. Phys. Chem B, **106** (2002) 8161
[19] N. D. Lang, Phys. Rev. B **34** (1986) 5947
[20] C. J. Chen, Phys. Rev. B **42** (1990) 8841
[21] W. A. Hofer, A. J. Fisher, R. A. Wolkow and P. Grütter, Phys. Rev. Lett. **87** (2001) 236104
[22] M. C. Desjonquéres and D. Spanjaard, Concepts in surface physics, Springer Verlag, Berlin (1996)
[23] R. T. Poole, J. G. Jenkin, J. Liesegang and R. C. G. Leckey, Phys. Rev. B **11** (1975) 5179
[24] Note that a proper notation of the overlayer with respect to the Cu(311) lattice can be phrased in matrix notation as (0 3; 1 1) for both structures[22]
[25] The slab contained six layers of Cu atoms. We used the same slab for the mono- and bi-layers, where a vacuum region corresponding to 17 Å for the bare Cu slab was used. For the trilayer, the vacuum region corresponded to 25 Å for the bare Cu slab. The surface unit cell contained three Cu atoms in each substrate layer and two Na and Cl atoms in each NaCl layer. The surface Brillouin zone (SBZ) was sampled using 36 k-points and the plane-wave cut-off energy was 300 eV.
[26] The atomic positions of the Na and Cl atoms and the first two layers of the Cu slab were allowed to relax while the remaining four Cu layers were fixed at their bulk equilibrium positions
[27] Experimentally measured band gap for bulk NaCl is 8.5 eV[23].
[28] Ultra violet photoemission and electron energy loss spectroscopy measurements by S. Fölsch (PhD thesis) showed a fully developed band gap of about 8.5eV for a bilayer on NaCl on Ge(100)